JOC The Journal of Organic Chemistry

Article

pubs.acs.org/joc

Through-the-Annulus Threading of the Larger Calix[8]arene Macrocycle

Carmine Gaeta,*[,†] Carmen Talotta,[†] Luigi Margarucci,[‡] Agostino Casapullo,[‡] and Placido Neri*[,†]

[†]Dipartimento di Chimica e Biologia, Università di Salerno, Via Giovanni Paolo II 132, I-84084 Fisciano, Salerno, Italy

[‡]Dipartimento di Farmacia, Università di Salerno, Via Giovanni Paolo II 132, I-84084 Fisciano, Salerno, Italy

Supporting Information

ABSTRACT: A complete study of the *through-the-annulus* threading of the larger calix[8]arene macrocycle with di-*n*-alkylammonium cations has been performed in the presence of the "superweak" TFPB counterion. Thus, it was found that such threading occurs only upon partial preorganization of the calix[8]arene macroring by intramolecular bridging. In particular, 1,5-bridged calix[8]arenes with a *meta*- or *para*-xylylene bridge (**2** and **3**) gave pseudo[2]rotaxanes in which one dialkylammonium axle (**4a**−**4e**$^+$) was threaded into one of the two subcavities of the calix[8]-wheel. Conformational studies by using chemical shift surface maps and DFT calculations evidenced a 3/4-cone geometry for these subcavities. Higher pseudorotaxane K_{ass} values were obtained for calix[8]-wheels **2** and **3**, with respect to calix[6]-host **1a**, due to the cooperative effect of their two subcavities. Dynamic NMR studies on calix[8]-pseudorotaxanes evidenced a direct correlation between K_{ass} (and ΔG_{ass}) values and energy barriers for calix inversion due to the effectiveness of thread templation. In accordance with DFT calculations, an *endo*-alkyl preference, over the *endo*-benzyl one, was observed by threading calix[8]-wheel **3** with the directional *n*-butylbenzylammonium axle **4d**$^+$.

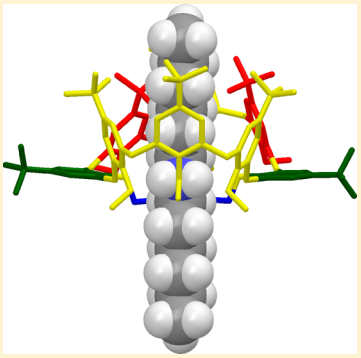

INTRODUCTION

In the last two decades, there has been a steeply increasing research interest in mechanically interlocked molecules (MIMs),[1] such as rotaxanes, catenanes, and knots, because of their applications in nanotechnology,[2] molecular machinery,[3] and sensing.[4] Interlocked architectures can be efficiently obtained through a template-directed synthesis[1,5] by exploiting the threading of a linear axle through a macrocyclic wheel to form a pseudorotaxane architecture, which can be considered the logical precursor to both catenanes and rotaxanes. Various kinds of macrocycles, including crown-ethers,[2,6] cyclodextrins,[7] cucurbiturils,[8] and macrolactams,[9] have been used as the basic wheel undergoing threading with a complementary axle component and exploiting various preorganizing supramolecular interactions.

Thanks to their synthetic versatility, calixarene macrocycles[10,11] have become one of the leading host systems, currently most studied in the context of anion[12] and cation recognition,[13] gas storage,[14] and self-assembly, both in solution[15] and in the solid state.[16] In contrast, their use as basic wheels in the construction of MIMs has been relatively limited[17] probably because of the lack of an efficient and general cavity-threading method.[18] In fact, this problem has been solved only very recently[19] by exploiting the inducing effect of the weakly coordinating Tetrakis[3,5-bis(tri-Fluoromethyl)Phenyl]Borate (TFPB$^-$) "superweak anion",[20] which allowed the first example of *through-the-annulus* threading of large calix[6]arene macrocycles with dialkylammonium cations. Thus, by means of this "superweak anion approach", we have obtained the first examples of calixarene-based [2 and 3]rotaxane[18] and [2]catenane[17a] interlocked architectures.

Literature data reported by us[19] and by Pappalardo and coworkers[21] have demonstrated that the *through-the-annulus* threading with secondary dialkylammonium ions can be observed both for 24-membered calix[6]arenes[19] and for 20-membered calix[5]arenes,[21] whereas the 18-membered dihomooxacalix[4]arene macroring cannot give it because of its small dimension.[20g] Currently, no information is available for the larger 32-membered calix[8]arene[22] macrocycle. Thus, prompted by these considerations, we decided to study the threading of scarcely functionalized calix[8]arene derivatives (**1b**, **2**, and **3**) with secondary dialkylammonium cations (**4a**−**4d**) in the presence of the superweak TFPB anion (Chart 1), and we report here the results of these studies.

RESULTS AND DISCUSSION

Threading Studies with Octamethoxy-*p*-*tert*-butylcalix[8]arene 1b. In a first attempt, we decided to test the complexing abilities toward dialkylammonium guests of the simple octamethyl ether of *p*-*tert*-butylcalix[8]arene (**1b**, Chart1).[23] In contrast with the analogous calix[6]arene hexamethyl-ether **1a** (Chart 1), we found that octamethoxycalix[8]arene **1b** gave no appreciable interactions upon titration with TFPB$^-$ salts of organic ammonium cation **4a**$^+$ (Figure 1).[24] This different behavior can be ascribed to the lower preorganization of the larger annulus of calix[8]arene **1b** with

Received: June 4, 2013
Published: July 9, 2013

   dx.doi.org/10.1021/jo401206j | *J. Org. Chem.* 2013, 78, 7627−7638

Chart 1

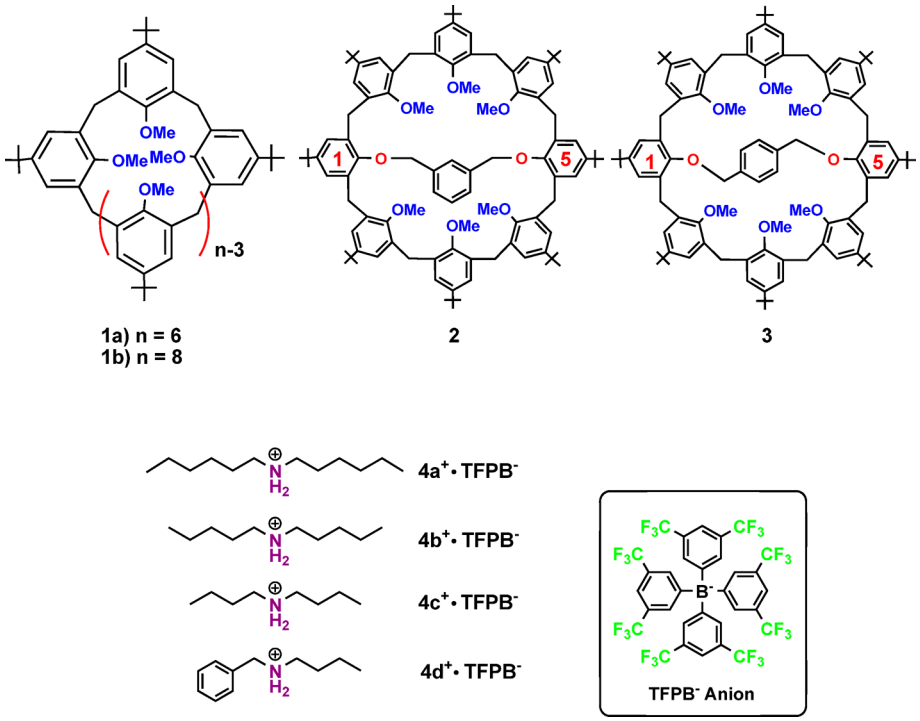

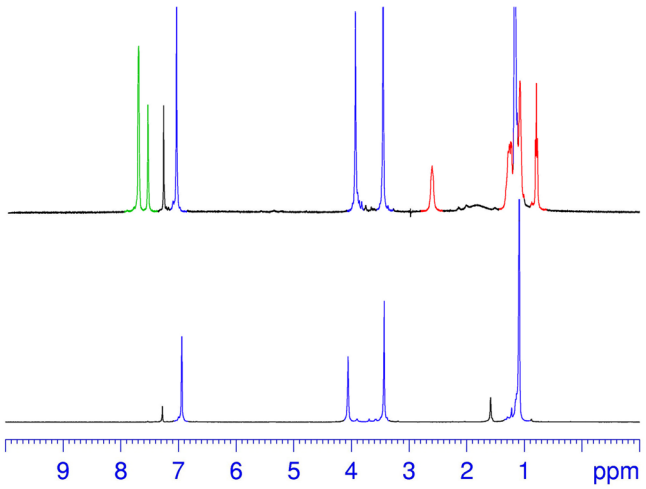

Figure 1. ^{1}H NMR spectra (400 MHz, $CDCl_3$, 298 K) of (bottom) **1b** and (top) equimolar solution (3 mM) of **1b** and **4a**$^+$·TFPB$^-$. In blue, red, and green, the ^{1}H NMR signals relative to **1b**, dihexylammonium cation **4a**$^+$, and TFPB$^-$ anion, respectively.

respect to the analogous calix[6]arene **1a**. In fact, it is well-known that, by increasing the number *n* of calix[*n*]arene aryl rings, a higher conformational mobility is observed, which is associated with an exponentially increasing number of calix conformations.[25]

As widely reported in the literature, the recognition abilities of larger calix[*n*]arenes (*n* = 6, 7, and 8) can be enhanced by hindering their conformational mobility through intramolecular bridging[20f] to give more preorganized shapes.[22,26] On this basis, we focused our attention to easily obtainable 1,5-monobridged-calix[8]arene derivatives **2** and **3**, bearing, respectively, a *meta*- or *para*-xylylene bridge[27] at the *endo* rim of the calix[8]arene macrocycle. This 1,5-bridging originates two identical subunits, each defined by three aromatic rings and a common portion, the bridge and the bridgehead rings. The two subunits of **2** and **3** are 24- and 25-membered macrorings, respectively, whose dimensions are very similar to those found in 24-membered calix[6]arene derivatives (e.g., **1a**).

Threading of 1,5-*m*-Xylylene-Bridged Calix[8]arene 2 with Di-*n*-hexylammonium Axle 4a$^+$. Interestingly, the addition of 1 equiv of di-*n*-hexylammonium salt **4a**$^+$·TFPB$^-$ to a $CDCl_3$ solution of 1,5-*m*-xylylene-bridged calix[8]arene host **2** caused dramatic changes in its ^{1}H NMR spectrum (Figure 2, spectra a and b). The most evident ones were the appearance of *n*-alkyl resonances in the upfield negative region of the spectrum (−0.22 and −1.13 ppm) and the formation of well-defined AX systems for $ArCH_2Ar$ groups (at 4.57/3.78, 4.65/3.56, 4.27/3.78, and 4.04/3.44 ppm; see also the COSY-45 spectrum in Figure 3), which are a clear indication that the di-*n*-hexylammonium axle **4a**$^+$ gave a *through-the-annulus*-threading with calix[8]arene host **2** in $CDCl_3$. In fact, the $ArCH_2Ar$ protons appear as a broad singlet for the conformationally mobile free host **2**, whereas they give rise to a couple of doublets (AX system) when the wheel is conformationally blocked by pseudorotaxane formation. In addition, the ESI(+) mass spectrum of the 1:1 mixture of **4a**$^+$·TFPB$^-$ and **2** gave a value of 1669.3 *m*/*z* as the base peak (Figure 2, spectrum c), corresponding to pseudo[2]rotaxane ion **4a**$^+$⊂**2** with a 1:1 host/guest stoichiometry, in which only one dialkylammonium axle was threaded into one of the two 24-membered subcavities of **2**. This stoichiometry was confirmed by integration of the slowly exchanging ^{1}H NMR signals of the pseudorotaxane complex.

Interestingly, scalar *J*-couplings were observed in the COSY-45 spectrum (Figure 3) of the above 1:1 mixture of **4a**$^+$·TFPB$^-$/**2** (400 MHz, $CDCl_3$, 298 K) between the dialkyl-NH_2^+ ammonium protons (6.31 ppm) and their *N*-linked *α* (1.33 ppm) and *α*′ (3.16 ppm) methylene groups, making straightforward the entire assignment of guest resonances. Thus, two different hexyl chains were clearly observed in the complex **4a**$^+$⊂**2**: one strongly shielded and inside the cavity (with

dx.doi.org/10.1021/jo401206j | J. Org. Chem. 2013, 78, 7627−7638

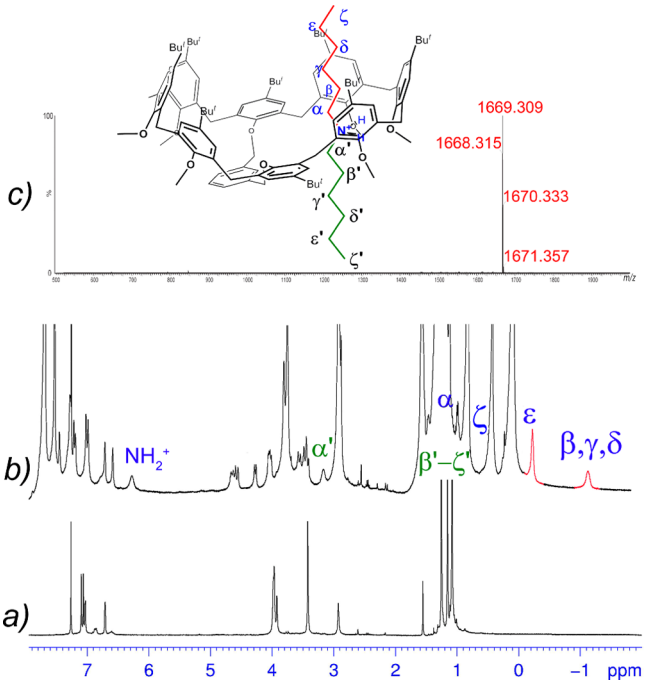

Figure 2. ^{1}H NMR spectra (400 MHz, $CDCl_3$, 298 K) of (a) **2** and (b) equimolar solution (3 mM) of **2** and **4a**$^+$·TFPB$^-$. (c) ESI(+) mass spectrum of an equimolar solution (3 mM) of **2** and **4a**$^+$·TFPB$^-$.

ζ, ε, δ, γ, β, and α protons resonating at 0.45, −0.22, −1.13, −1.13, −1.13, and 1.33 ppm, respectively) and the other, at more normal values of chemical shift (with ζ', ε', δ', γ', β', and α' protons resonating at 0.93, 0.88, 0.82, 1.25, 1.60, and 3.16 ppm, respectively), outside the cavity. Interestingly, a further inspection of the COSY-45 spectrum revealed the presence of 5 AX systems (see inset in Figure 3) at 4.57/3.78, 4.65/3.56, 4.27/3.78, and 4.04/3.44 (2 overlapped AX systems) ppm relative to four calixarene $ArCH_2Ar$ groups and to one OCH_2 group of the *m*-xylylene bridge, which are consistent with a C_{2v} calix[8]arene structure possessing a symmetry plane orthogonal to the 1,5-*m*-xylylene bridge and bisecting the two opposite 3,7-calixarene aromatic rings. Naturally, the presence of this symmetry plane is compatible with the 1:1 axle/wheel stoichiometry of the pseudo[2]rotaxane structure. In a 2D ROESY spectrum (400 MHz, $CDCl_3$, 298 K), the **4a**$^+$⊂**2** pseudo[2]rotaxane gives rise to diagnostic ROE correlations among the shielded ε signal at −0.22 ppm and the host $ArCH_2Ar$ protons at 4.04/3.47 and 4.57/3.78 ppm (Figure S6, top, Supporting Information). In addition, a cross-peak was also present between ε protons of the thread **4a**$^+$ and the *tert*-butyl singlet of **2** at 1.37 ppm (Figure S6, bottom, Supporting Information). The spatial proximity of wheel **2** and axle **4a**$^+$ was also confirmed by two diagnostic ROE cross-peaks among the shielded β, γ, and δ overlapped signals at −1.13 ppm and the calixarene ArH protons at 7.28 and 7.51 ppm (Figure S5, bottom, Supporting Information).

To obtain further insights about the conformation adopted by **2** in pseudo[2]rotaxane **4a**$^+$⊂**2**, further studies were undertaken. Of course, the calix[8]arene macrocycle presents high conformational complexity, as testified by the different conformations (such as the *pleated-loop*[28] or *chairlike*[29,30] ones) obtained by X-ray crystallography. Consequently, we decided to resort to the novel method previously proposed by us for the assessment of calixarene conformations based on the QM GIAO calculation of ^{13}C and ^{1}H NMR chemical shift values of $ArCH_2Ar$ groups.[31] The validity of this method was recently confirmed by the similarity between predicted and experimental X-ray structures

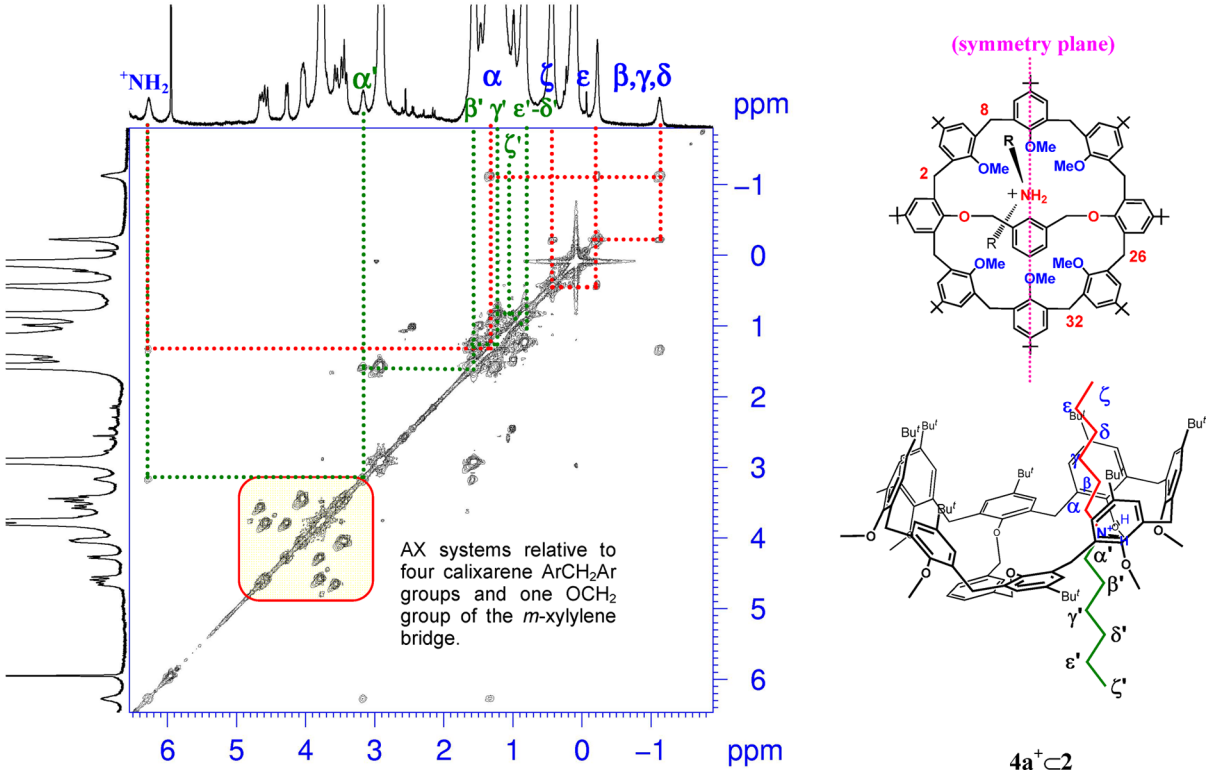

Figure 3. Portion of the COSY-45 spectrum (400 MHz, $CDCl_3$, 298 K) of an equimolar solution (3 mM) of **2** and **4a**$^+$·TFPB$^-$.

dx.doi.org/10.1021/jo401206j | J. Org. Chem. 2013, 78, 7627−7638

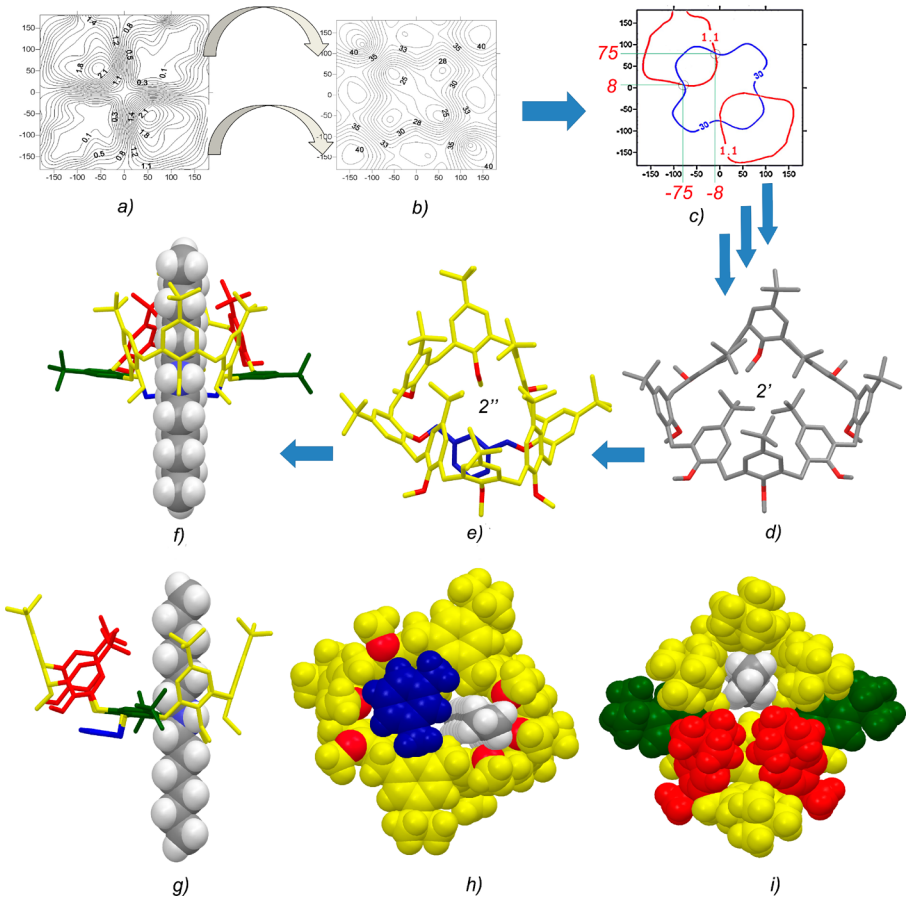

Figure 4. Contour plot representations of the ^{1}H $\Delta\delta$ (a) and ^{13}C δ (b) chemical shift values (ppm) of the $ArCH_2Ar$ group versus the ϕ and χ torsion angles. (c) Computer-assisted graphical superimposition of the lines relative to experimental ^{1}H $\Delta\delta$ = 1.1 ppm and ^{13}C = 30.0 ppm values for methylene group C-26 (or C-44) (Table 1); the other lines of the countour plots (a) and (b) have been omitted for clarity. (d) Crude model (Maestro 4.1) **2′** obtained by imposing the ϕ and χ torsion angle values reported in Table 1 on the calix[8]arene skeleton of **2**. (e) Lowest MM3 energy conformation **2″** (MacroModel 9.0, $CHCl_3$ GB/SA implicit model solvent) obtained from crude model **2′**. (f) Energy-minimized structure of pseudo[2]rotaxane **4a**$^{+}$⊂**2** (B3LYP DFT calculations using the 6-31G* basis set) obtained starting from **2″**. (g) Side view of the DFT-energy-minimized structure of pseudo[2]rotaxane **4a**$^{+}$⊂**2**. (h) Bottom and (i) top views of the CPK model of the DFT-energy-minimized structure of **4a**$^{+}$⊂**2** pseudo[2]rotaxane.

of a calix[7]arene derivative.[20f] In particular, following the reported indications, we used the published chemical shift surface maps in which the ^{1}H $\Delta\delta$ (Figure 4a and Figure S27, Supporting Information) and ^{13}C δ (Figure 4b and Figure S28, Supporting Information) values of the calixarene $ArCH_2Ar$ groups are correlated with the ϕ and χ torsion angles of the Ar−CH_2−Ar bonds.

Thus, the simultaneous fitting of experimental ^{1}H $\Delta\delta$ and ^{13}C δ values obtained by superimposition of the relative maps (Figure 4c) allowed us to obtain a series of possible combinations of ϕ and χ torsion angles of the Ar−CH_2−Ar bonds (Table 1).

To apply this strategy, a complete assignment for both ^{1}H and ^{13}C NMR signals of **4a**$^{+}$⊂**2** pseudo[2]rotaxane was obtained at room temperature by means of a detailed 1D and 2D NMR study (COSY-45, HSQC, and HMBC spectra, 400 MHz, $CDCl_3$).

Consequently, for each pair of symmetry-equivalent methylene groups [at positions 2(20), 8(14), 26(44), and 32(38); see Table 1], the simultaneous fitting of the corresponding pair of experimental ^{1}H $\Delta\delta$ and ^{13}C δ values (Table 1) in the contour plots (Figure 4a−c) was obtained through computer-assisted graphical superimposition (see Figure 4c) of the relative ^{1}H $\Delta\delta$ and ^{13}C δ lines. As an example, Figure 4c illustrates the case of the methylene group at position 26 (or 44): ^{1}H $\Delta\delta$ = 1.1 ppm and ^{13}C δ = 30.0 ppm. Thus, through the coordinates of each intersection point, we obtained the ϕ and χ torsion angles values of +75/−8.0 and −75/+8.0. By repeating this procedure for the remaining positions, we obtained the ϕ and χ torsion angle values reported in Table 1. These data were then used in a modeling program[32] (Maestro 4.1) to build the possible conformer starting with an open-chain calix[8]arene skeleton. The first and obvious criterion followed to select the compatible conformers was to discard those arrangements that lack the closure of the calix[8]arene macrocycle (see Figures S26−S31, Supporting Information). In this way, only the following sequence of torsion angle values was obtained for the first half of the macrocycle (see also Figure S30, Supporting Information): +10/+50 (C38), +8/−75 (C44), −7.5/−85 (C2), and +73/0.0 (C8). Values with opposite signs (mirror image) were obtained for the second one: −73/0.0 (C14), +7.5/+85 (C20), −8/+75 (C26), and −50 /−10 (C32). Thus, from this sequence of torsion angle values, the crude model **2′** was built (see Figure 4d). Crude model **2′** displays all calixarene oxygen atoms on the same side of the molecule, with the two bridged rings A and E "outward" inclined to permit the *m*-xylylene bridging. Refinement of the crude model **2′** was obtained through molecular mechanics calculations[32] (MM3 Force Field, $CHCl_3$ GB/SA implicit model solvent), and the energy-minimized structure **2″** (Figure 4e) was used as starting host-structure for the successive **4a**$^{+}$⊂**2**

dx.doi.org/10.1021/jo401206j | J. Org. Chem. 2013, 78, 7627−7638

Table 1. ϕ and χ Torsion Angles of Calix[8]arene Wheel 2 in Pseudo[2]rotaxane $4a^+\subset 2$ Derived by Chemical Shift Surface Maps (^{13}C δ and ^1H $\Delta\delta$) for $ArCH_2Ar$ Groups

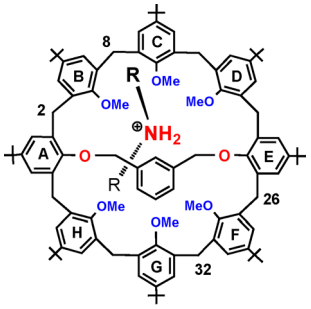

$4a^+\subset 2$

position	C(2) or C(20)	C(8) or C(14)	C(26) or C(44)	C(32) or C(38)
^{13}C δ^a (ppm)	32	30	30	27
^1H $\Delta\delta^a$ (ppm)	0.57	0.80	1.10	0.6
ϕ and χ (deg)	(−7.5/−85)	(0.0/−73)	(−8.0/+75)	(−10/−50)
	(+7.5/+85)	(0.0/+73)	(+8.0/−75)	(+10/+50)

[a]The complete NMR signal assignment leading to $\Delta\delta$ ^1H and ^{13}C δ values for the methylene groups of **2** in pseudo[2]rotaxane $4a^+\subset 2$ was obtained by means of a detailed 1D and 2D NMR spectroscopy study (COSY, HSQC, and HMBC 2D NMR spectra, 400 MHz, $CDCl_3$, 298 K). ^1H $\Delta\delta$ values were calculated as the distance on the ppm scale between the two doublets of the AX system of each $ArCH_2Ar$ group of **2** in pseudo[2]rotaxane $4a^+\subset 2$.

pseudo[2]rotaxane construction. The lowest-energy structure of the $4a^+\subset 2$ pseudo[2]rotaxane thus obtained was optimized by DFT calculations[33] at the B3LYP/6-31G* level of theory (Figure 4f–i), which evidenced two strongly stabilizing, bifurcated N–H···O hydrogen bonds. A closer inspection of the optimized structure of the $4a^+\subset 2$ pseudo[2]rotaxane (Figure 4f–i) allowed us to attribute the cone relationship to the contiguous triads of anisole rings (B–C–D and F–G–H rings in Table 1) in **2**. Therefore, both triads adopt a 3/4-cone geometry, whereas an out orientation is assumed by the bridgehead A and E rings (see Table 1). On this basis, the two subunits of calix[8]arene **2** adopt a "*syn*-cones" orientation in the $4a^+\subset 2$ pseudo[2]rotaxane structure. A further inspection of the CPK model of the $4a^+\subset 2$ pseudo[2]rotaxane structure (see Figure 4h) revealed that the aromatic *m*-xylylene bridge (blue colored in Figure 4h) is positioned right at the bottom of the free subcavity of **2**, thus obstructing both the *oxygen-* and the *tert-butyl-through-the-annulus* passages. This is in accordance with the presence of two AX systems for 26(44) and 32(38) $ArCH_2Ar$ groups of the unthreaded subcavity of **2** (4.65/3.56 and 4.05/3.43 ppm), which is a clear indication that this subcavity is blocked in the NMR time scale in a cone conformation,[34] though it is not threaded. Interestingly, the DFT-optimized structure of pseudo[2]-rotaxane $4a^+\subset 2$ revealed that the *t*Bu groups of F and H anisole rings (see red color in Figure 4i) of the unthreaded 3/4-cone subunit are inward oriented to give a self-inclusion of these groups inside the calix cavity.

Titration experiments, in which the concentration of **2** was kept constant while the concentration of axle $4a^+$ was varied, confirmed the 1:1 stoichiometry of pseudo[2]rotaxane $4a^+\subset 2$ even after the addition of a large excess of $4a^+$. The inspection of the CPK model of the $4a^+\subset 2$ pseudo[2]rotaxane (Figure 4h,i) corroborated this result. In fact, the presence of axle $4a^+$ into the first subcavity of **2** forces the *m*-xylylene bridge to close the gateway to the second subunity of **2** (see Figure 4h).

Finally, a quantitative[35] ^1H NMR experiment led to an apparent association constant for the slowly exchanging $4a^+\subset 2$ pseudo[2]rotaxane of 3400 ± 300 M^{-1}, which is suprisingly higher than that observed for the analogous complexation of $4a^+$ with calix[6]arene host **1a** (2700 ± 200 M^{-1}).[19] In fact, a competition experiment (Figure 5) was performed by treating 1

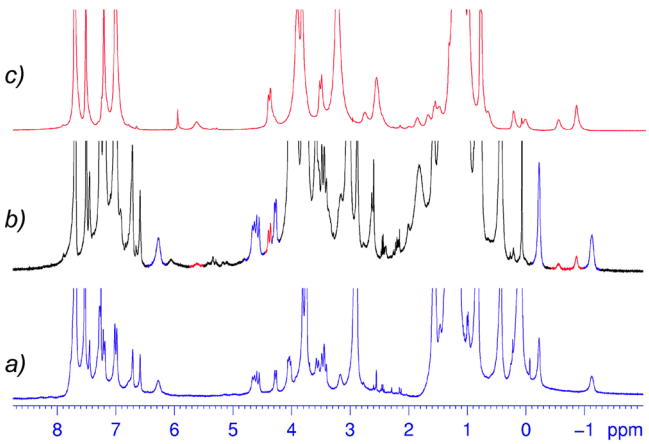

Figure 5. ^1H NMR spectra (400 MHz, $CDCl_3$, 298 K) of (a) equimolar solution (3 mM) of **1a** and $4a^+\cdot TFPB^-$, (b) equimolar solution of **1a**, **2**, and $4a^+\cdot TFPB^-$ (3 mM each), and (c) equimolar solution (3 mM) of **2** and $4a^+\cdot TFPB^-$.

equiv of $4a^+$ in $CDCl_3$ with a mixture of the two different hosts **1a** and **2** (1 equiv each). Thus, it was evidenced that $4a^+\subset 2$ is preferentially formed over $4a^+\subset 1a$ in a ratio of 7:3 (Figure 5), probably because of the cooperative[36] action of the two 3/4-cone subcavities in the threading process. Interestingly, the upfield shift experienced by α protons of guest $4a^+$ into the cavity of calix[8]-wheel **2** ($\Delta\delta$ = 1.61 ppm) is significantly lower with respect to that observed for the analogous protons into the narrower cavity of calix[6]-wheel **1a** ($\Delta\delta$ = 2.30 ppm). Differently, ε, δ, γ, and β protons in pseudo[2]rotaxane $4a^+\subset 2$ experienced an upfield shift ($\Delta\delta$ = 1.46, 2.37, 2.37, and 2.65 ppm, respectively) higher with respect to that observed for the analogous protons of $4a^+\subset 1a$ ($\Delta\delta$ = 1.27, 1.74, 2.06, and 2.34

dx.doi.org/10.1021/jo401206j | J. Org. Chem. 2013, 78, 7627–7638

ppm, respectively). A closer inspection of the DFT-calculated structures of **4a**$^+$⊂**2** and **4a**$^+$⊂**1a** (Figure 6) revealed that thread

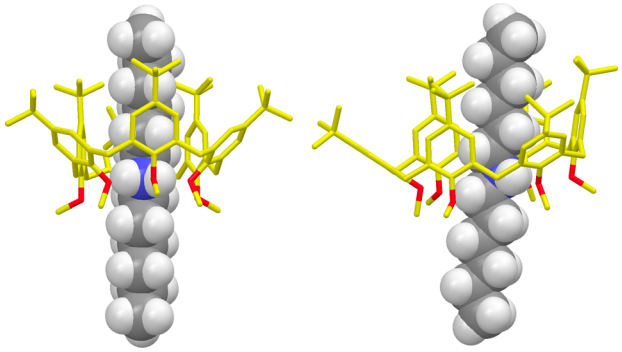

Figure 6. Front (left) and side (right) views of the energy-minimized structure of pseudo[2]rotaxane **4a**$^+$⊂**1a** (B3LYP DFT calculations using the 6-31G* basis set).

4a$^+$ penetrated more deeply into the 3/4-cone subcavity of **2**. In fact, the NH_2^+ and α protons of guest **4a**$^+$ were sitting at a distance of 0.29 and 1.45 Å, respectively, above the mean plane of calixarene oxygen atoms of the 3/4-cone subcavity of **2**, a value significantly lower with respect to that observed for the analogous protons of **4a**$^+$⊂**1a** (0.52 and 1.90 Å, respectively).

Threading of 1,5-*p*-Xylylene-Bridged Calix[8]arene 3 with Di-*n*-hexylammonium Axle 4a$^+$. At this point, it is interesting to study the binding abilities of 1,5-*p*-xylylene-bridged calix[8]arene derivative **3** in which two 25-membered subcavities are now delimited by the *p*-xylylene bridge (Figure 7). With

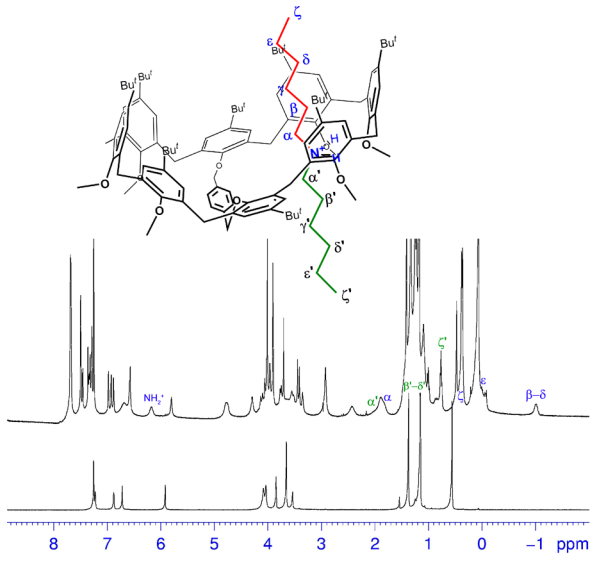

Figure 7. ^{1}H NMR spectra (400 MHz, $CDCl_3$, 298 K) of (bottom) **3** and (top) equimolar solution (3 mM) of **3** and **4a**$^+$·$TFPB^-$.

respect to derivative **2**, containing two *m*-xylylene-bordered 24-membered subcavities, calix[8]arene **3** gave the *through-the-annulus* threading with di-*n*-hexylammonium axle **4a**$^+$ with an association constant of 8400 ± 400 M^{-1}, a value significantly higher than that observed for **2** (3400 ± 300 M^{-1}; selectivity ratio = K_{ass}(**4a**$^+$⊂**3**)/K_{ass}(**4a**$^+$⊂**2**) = 2.5). Again, the ESI(+) mass spectrum of a 1:1 mixture of **4a**$^+$·$TFPB^-$ and **3** (Figure S2, bottom, Supporting Information) gave a value of 1669.3 *m*/*z* as the base peak, corresponding to pseudo[2]rotaxane ion **4a**$^+$⊂**3** with a 1:1 host/guest stoichiometry, in which only one dialkylammonium axle was threaded into one of the two 25-membered subcavities of **3**. As above, a COSY-45 spectrum (Figure S12, Supporting Information) allowed a complete confident assignment of all *n*-alkyl resonances of the axle of pseudo[2]rotaxane **4a**$^+$⊂**3**. Naturally, two different hexyl chains were also observed here: one strongly shielded inside the cavity (with ζ, ε, δ, γ, β, and α protons resonating at 0.47, −0.01, −1.01 (3 × 2H), and 1.82 ppm, respectively) and the other unshielded outside the cavity (with ζ', ε', δ', γ', β', and α' protons resonating at 0.78, 0.74, 0.99, 1.44, 1.39, and 1.90 ppm, respectively).

The higher association constant of **4a**$^+$⊂**3** over **4a**$^+$⊂**2** can be explained by the larger dimension of the 25-membered subcavity of **3**, over the 24-membered one of **2**, which would give a better accommodation of the axle. In addition, a role could be also played by the less symmetrical nature of the *m*-bridge in **2**, over the linear *p*-bridge of **3**, which could give an additional sterical hindrance with its ArH in *ortho* to the bridgehead carbons.

Regarding the upfield shift experienced by α protons of guest **4a**$^+$ upon threading into the cavity of calix[8]-wheel **3**, a value of 1.12 ppm was found, which is slightly lower than that of **4a**$^+$⊂**2** ($\Delta\delta$ = 1.61 ppm), but significantly lower than that of **4a**$^+$⊂**1a** ($\Delta\delta$ = 2.30 ppm). As above, these data can be well-explained in terms of a deeper axle penetration in **4a**$^+$⊂**3**. Instead, quite more surprising was the finding that α' protons of guest **4a**$^+$ outside the cavity of calix[8]-wheel **3** also experienced an *upfield shift* ($\Delta\delta = \delta_{complexed} - \delta_{free} = 1.90 - 2.94 = -1.04$ ppm. In sharp contrast, the analogous α' protons in **4a**$^+$⊂**2** gave an unexpected *downfield shift* ($\Delta\delta = \delta_{complexed} - \delta_{free} = 3.16 - 2.94 = 0.22$ ppm).

These contrasting data can be explained by a closer inspection of the DFT-calculated structure of pseudo[2]rotaxane **4a**$^+$⊂**3** (Figure 8a), which revealed that the aromatic ring of the *p*-xylylene bridge of **3** adopts an almost perpendicular orientation with respect to the calix cavity (Figure 8c,d). In this way, the α' protons of guest **4a**$^+$ outside the cavity (in magenta in Figure 8d) became in close contact with the *p*-xylylene ring (*p*-xylylene-ring-centroid/α' protons distance = 3.56 Å) and fall in its aromatic

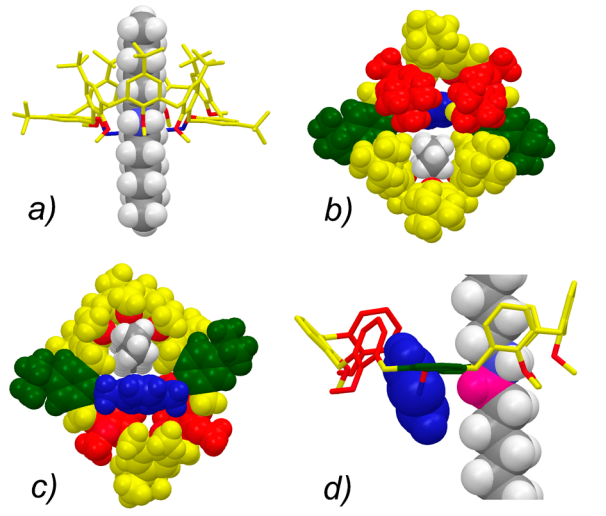

Figure 8. Energy-minimized structures of pseudo[2]rotaxane **4a**$^+$⊂**3** (B3LYP DFT calculations using the 6-31G* basis set): (a) Front view. (b) Top and (c) bottom views of the CPK model (in blue, the *p*-xylylene bridge). (d) Detailed view of the orientation of the *p*-xylylene bridge (CPK in blue) with respect to the calixarene cavity and thread **4a**$^+$ (H atoms and *t*-Bu groups of the calixarene skeleton have been omitted for clarity).

dx.doi.org/10.1021/jo401206j | J. Org. Chem. 2013, 78, 7627−7638

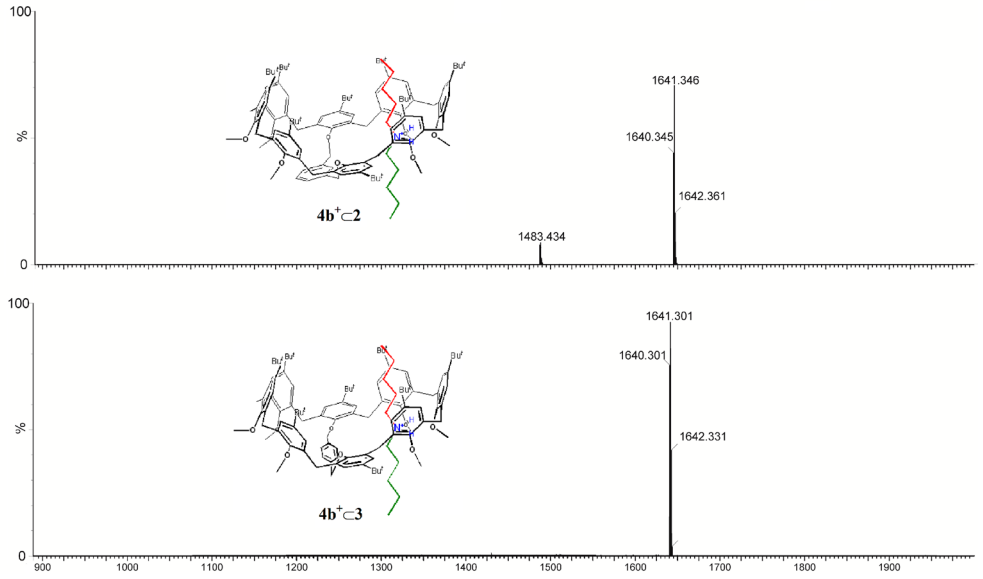

Figure 9. ESI(+) mass spectra of equimolar solutions (3 mM) of (top) **4b**$^+$·TFPB$^-$ and **2**, and (bottom) **4b**$^+$·TFPB$^-$ and **3**.

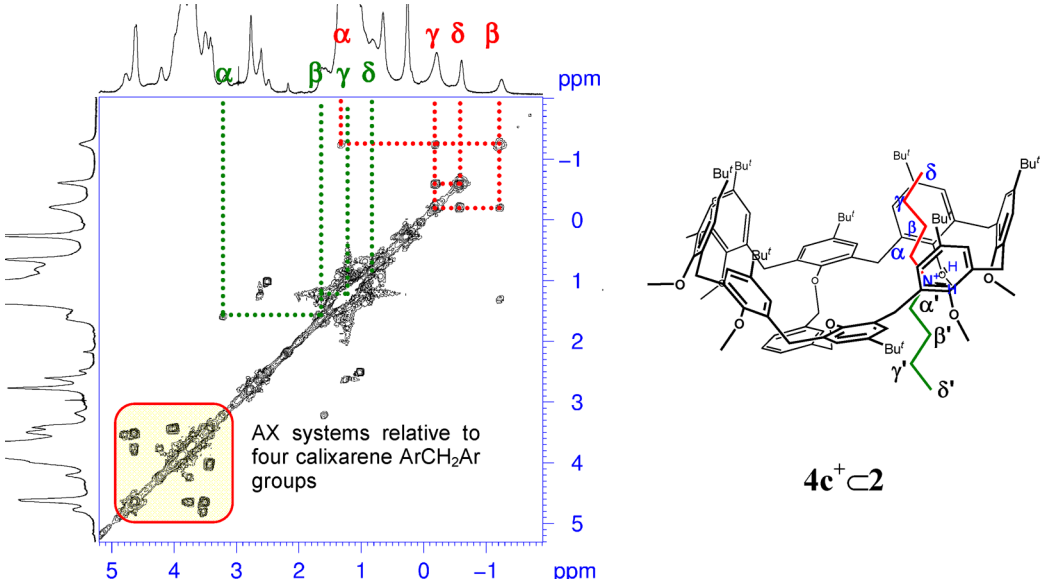

Figure 10. Portion of the COSY-45 spectrum (400 MHz, $CDCl_3$, 223 K) of an equimolar solution (3 mM) of **2** and di-*n*-butylammonium **4c**$^+$·TFPB$^-$.

shielding cone to give the observed 1.04 ppm *upfield shift*. In a similar way, the inspection of the DFT-optimized structure of pseudo[2]rotaxane **4a**$^+$⊂**2** (Figure 4h) revealed that the analogous *exo*-cavity α′ protons of guest **4a**$^+$ are facing the ArH proton of the horizontal *m*-xylylene ring and fall in its aromatic deshielding zone to give the observed 0.22 ppm *downfield shift*.

In analogy to **4a**$^+$⊂**2** (Figure 4h), the CPK model of **4a**$^+$⊂**3** (Figure 8c) revealed that the presence of axle **4a**$^+$ into the first subcavity of **3** forces the *p*-xylylene bridge to close the gateway to the second subunity of **3**, corroborating in this way the 1:1 stoichiometry observed even in the presence of a strong excess of cation **4a**$^+$. In addition, the optimized structure of **4a**$^+$⊂**3** revealed that the *t*Bu groups of F and H anisole rings (see red color in Figure 8b) of the unthreaded 3/4-cone subunit are inward oriented to give their self-inclusion inside the calix cavity.

Threading of 2 and 3 with Di-*n*-pentylammonium Axle 4b$^+$. The extension of ^{1}H NMR complexation studies (Figures S14 and S15, Supporting Information, 400 MHz, $CDCl_3$, 298 K) to di-*n*-pentylammonium ion **4b**$^+$ revealed again spectral changes similar to those discussed above, with the appearance of upfield resonances pertinent to the *n*-pentyl chain inside the aromatic cavity of **2** (Figure S14, Supporting Information). A base peak at 1641.3 *m*/*z* in the ESI(+) mass spectrum in Figure 9 (top) confirmed the formation of the **4b**$^+$⊂**2** complex. A ^{1}H NMR spectrum of the 1:1 titration mixture of **4b**$^+$ and **2** in $CDCl_3$ showed slowly exchanging signals for both free and complexed host; thus, a quantitative ^{1}H NMR experiment led to an apparent association constant for pseudo[2]rotaxane **4b**$^+$⊂**2** of 1700 ± 200 M^{-1}.

Similar results were obtained in the threading of *p*-xylylene-bridged **3** (Figure S15, Supporting Information) with di-*n*-pentylammonium axle **4b**$^+$ to give a K_{ass} value of 2100 ± 200 M^{-1}. Once again, the cooperative[36] action of the two 3/4-cone subcavities in the threading process between **4b**$^+$ and **2** or **3** led to K_{ass} values significantly higher than that reported for calix[6]-

dx.doi.org/10.1021/jo401206j | J. Org. Chem. 2013, 78, 7627−7638

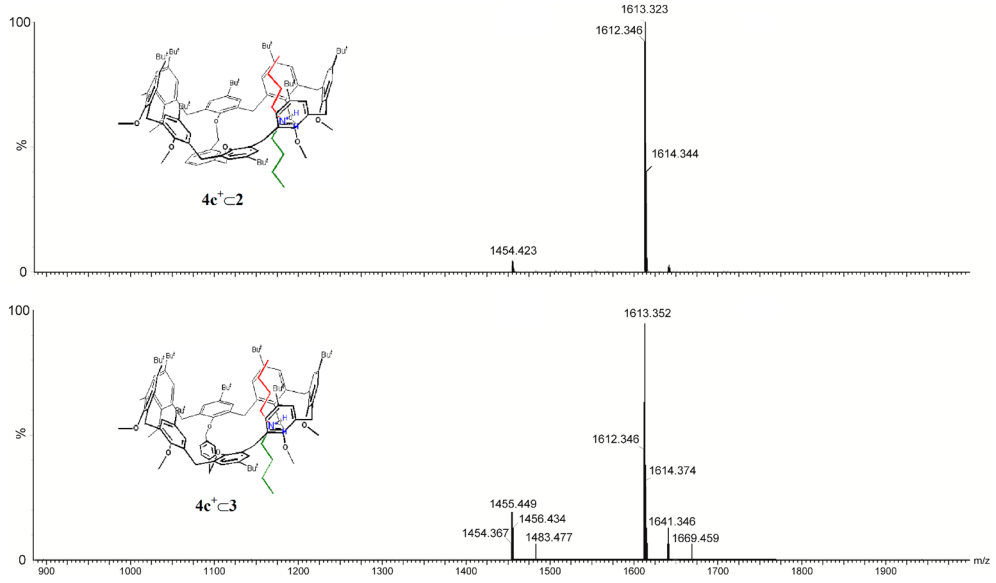

Figure 11. ESI(+) mass spectra of equimolar solutions (3 mM) of (top) **4c**$^+$·TFPB$^-$ and **2**, and (bottom) **4c**$^+$·TFPB$^-$ and **3**.

arene host **1a** (440 M^{-1}).[19] As above, also in this instance, a higher stability was observed for **4b**$^+$⊂**3** over **4b**$^+$⊂**2**.

Threading of 2 and 3 with Di-*n*-butylammonium Axle 4c$^+$. Surprisingly, the addition of di-*n*-butylammonium axle **4c**$^+$ to a $CDCl_3$ solution of **2** (400 MHz, 298 K) caused a broadening of the host signals. Lowering the temperature at 248 K caused a decoalescence of calix $ArCH_2Ar$ signals into four AX systems at 4.80/3.50, 4.64/3.51, 4.63/3.77, and 3.99/3.43 ppm (see inset in the COSY-45 spectrum in Figure 10), in agreement with the freezing of the two subcavities of **2** in the 3/4-cone conformation. As above, a COSY-45 spectrum (Figure 10) of the 1:1 mixture of **4c**$^+$ and **2** at 223 K ($CDCl_3$, 400 MHz) allowed a complete confident assignment of all *n*-butyl resonances of the axle of pseudo[2]rotaxane **4c**$^+$⊂**2**. Two different butyl chains were again observed, a strongly shielded *endo*-cavity one (with δ, γ, β, and α protons resonating at −0.57, −0.22, −1.25, and 1.31 ppm, respectively; see Figure 10), and the corresponding unshielded *exo*-cavity (with δ, γ, β, and α protons resonating at −0.57, −0.22, −1.25, and 1.31 ppm, respectively; see Figure 10).

A quantitative ^{1}H NMR study at 223 K revealed an apparent association constant of 190 ± 25 M^{-1} for **4c**$^+$⊂**2** pseudorotaxane. To confirm the pseudo[2]rotaxane formation, the ESI(+) mass spectrum of a 1:1 mixture of **4c**$^+$·TFPB$^-$ and **2** gave a value of 1613.3 *m*/*z* as the base peak (Figure 11, top), corresponding to the **4c**$^+$⊂**2** ion with a 1:1 host/guest stoichiometry.

A similar behavior was observed in the threading study of **4c**$^+$ with **3**, which led to an apparent association constant of 300 ± 40 M^{-1} at 223 K for pseudo[2]rotaxane **4c**$^+$⊂**3**. This confirmed the general trend of the higher pseudorotaxane stability of wheel **3** over **2**.

Dynamic NMR Studies. The temperature dependence observed with di-*n*-butylammonium axle **4c**$^+$ induced us to perform more detailed VT NMR studies. Thus, dynamic ^{1}H NMR studies (400 MHz, TCDE) evidenced a dethreading of axle **4c**$^+$ from pseudo[2]rotaxane **4c**$^+$⊂**2** at temperatures above 298 K, as indicated by the disappearance of shielded *n*-butyl resonances (Figure 12). Analogously, a coalescence was ascertained at 298 K for $ArCH_2Ar$ AX systems of **2**, which sharpened at 358 K (Figure 12) to two singlets, indicative of its fast conformational interconversion.

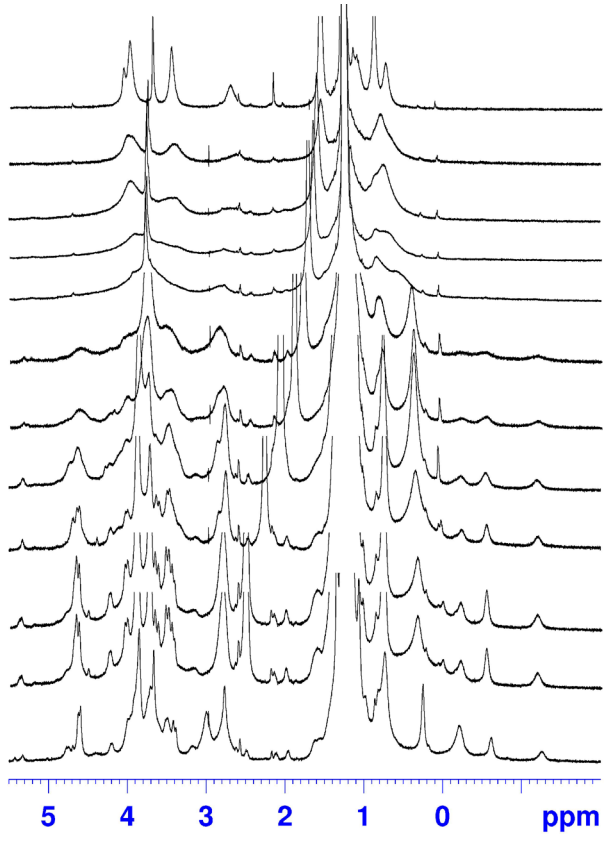

Figure 12. ^{1}H NMR spectra (400 MHz) of an equimolar solution (3 mM) of **2** and **4c**$^+$·TFPB$^-$, from bottom to the top: 223, 233, 243, 253, 263, 273, 283, 298, 308, 318, 328 ($CDCl_3$ as solvent), and 358 K (TCDE as solvent).

From these data, an energy barrier of 13.7 kcal/mol for calix conformational interconversion was estimated. Similar studies (400 MHz, TCDE) for dipentylammonium-based **4b**$^+$⊂**2** and dihexylammonium-based **4a**$^+$⊂**2** led to energy barriers ($\Delta G^{\ddagger}$) of 15.4 (T_c = 333 K) and 16.8 kcal/mol (T_c = 363 K), respectively (Table 2). In accordance with previous results,[19] these data confirm that, in larger-calixarene-based pseudorotaxane archi-

dx.doi.org/10.1021/jo401206j | J. Org. Chem. 2013, 78, 7627−7638

Table 2. Comparison between K_{ass}, ΔG_{ass}, and $\Delta G^{\ddagger}$ Obtained by ^{1}H VT NMR Studies (400 MHz)

	$4a^+\subset3$	$4a^+\subset2$	$4b^+\subset3$	$4b^+\subset2$	$4c^+\subset3$	$4c^+\subset2$
K_{ass} (M^{-1})[a]	8400	3400	2100	1720	300[b]	190[b]
$\Delta G^{\ddagger}$ (kcal/mol)	>17.4	16.8	15.8	15.4	14.9	13.7
T_c (K)	>383	363	353	333	323	298
ΔG_{ass} (kcal/mol)[c]	5.35	4.81	4.53	4.41	2.52[b]	2.32[b]

[a] K_{ass} were determined by quantitative ^{1}H NMR experiment (error < 15%). [b] Calculated at 223 K. [c] $\Delta G_{ass} = -RT \ln K_{ass}$. The calculated data have been reported in absolute value.

tectures, the ammonium templation of the thread has an important role in the stabilization of the conformation of the calix wheel. In fact, this conformational stabilization defined by the energy barrier value ($\Delta G^{\ddagger}$) can be compared with the ΔG_{ass} of complexation calculated from the experimental association constants (Table 2). Thus, increasing the thermodynamic stability (ΔG_{ass}) of the calixarene-based pseudorotaxane increases the conformational stabilities of the wheel ($\Delta G^{\ddagger}$).

In accordance with this conclusion was also the comparison of dibutylammonium-based **4c**$^+\subset$**3** and **4c**$^+\subset$**2** pseudo[2]rotaxanes. In fact, VT ^{1}H NMR led to an energy barrier of 14.9 kcal/mol for calixarene conformational interconversion (T_c = 323 K for $ArCH_2Ar$) of **4c**$^+\subset$**3** pseudo[2]rotaxane, which is higher with respect to that of **4c**$^+\subset$**2** pseudo[2]rotaxane (13.7 kcal/mol, T_c = 298 K), thus reflecting their different stability constants (K_{ass} = 300 and 190 M^{-1}, respectively) and ΔG_{ass} (2.52 and 2.32 kcal/mol, respectively).

Finally, pseudorotaxane **4a**$^+\subset$**3**, which presents the highest K_{ass} in the present study (8400 M^{-1}), showed no hint of coalescence for temperatures up to 383 K. Consequently, an energy barrier surely higher than 17.4 kcal/mol can be estimated for its conformational inversion (Table 2).

Directional Threading of 2 and 3 with *n*-Butylbenzylammonium Axle 4d$^+$. As a final point, we decided to study the threading of directional alkylbenzylammonium cation **4d**$^+$ with calix[8]arene hosts **2** and **3**. Generally, the threading of unsymmetrical threads with directional calixarene wheels would give rise to two stereoisomeric orientational pseudorotaxanes with an *endo*-alkyl or *endo*-benzyl cavity complexation (Figure 13).[19] Previuosly, we showed that the threading with calix[6]arene wheels leads to the preferential formation of *endo*-alkyl complexes over the *endo*-benzyl ones (Figure 13),[18b−d,19,37] and therefore, it is quite interesting to know the behavior of calix[8]arene hosts.

Surprisingly, the ^{1}H NMR spectrum of a mixture of the TFPB salt of butylbenzylammonium **4d**$^+$ and calix[8]arene wheel **2** in $CDCl_3$ showed no hint of threading even after addition of a large excess of axle or prolonged equilibration times (up to 72 h at 60 °C). Differently, when the benzylbutylammonium **4d**$^+$ cation was added to a $CDCl_3$ (Figure 14) solution of calix[8]arene

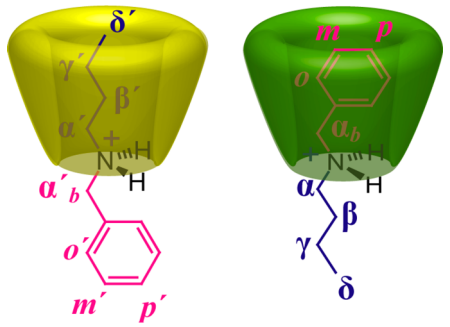

Figure 13. Cartoon representation of *endo*-alkyl (yellow) and *endo*-benzyl (green) oriented calixarene-based pseudo[2]rotaxanes.

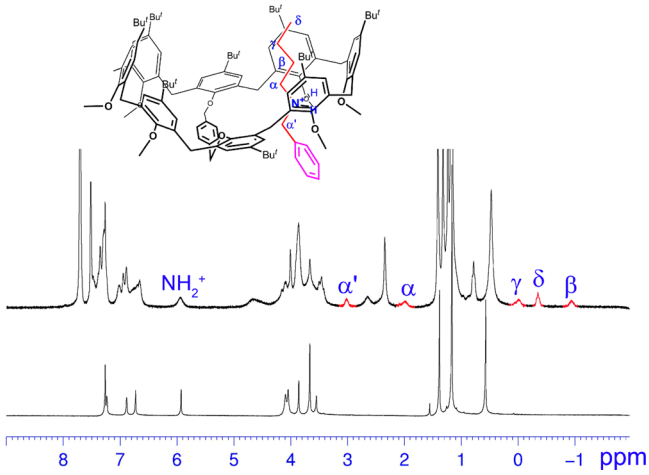

Figure 14. ^{1}H NMR spectra (400 MHz, $CDCl_3$, 298 K) of (bottom) **3**, and (top) equimolar solution (3 mM) of **3** and **4d**$^+$·TFPB$^-$.

wheel **3**, a clear threading was observed. The most evident NMR spectral changes were the appearance of *n*-alkyl resonances in the upfield negative region of the spectrum (−0.94 and 0.02 ppm) and the formation of well-defined AX systems for $ArCH_2Ar$ groups (see COSY-45 spectrum in Figure S22, Supporting Information),[24] which are a clear indication that the axle **4d**$^+$ gave a *through-the-annulus* threading with calix[8]arene host **3** in $CDCl_3$.

The pseudo[2]rotaxane formation was confirmed by a prominent peak at 1647.3 *m*/*z* in the ESI(+) mass spectrum, corresponding to the **4d**$^+\subset$**3** supramolecular ion (Figure S1, Supporting Information). Obviously, the presence of highfield shifted *n*-Bu signals in the ^{1}H NMR spectrum (Figure 14) is indicative of an an *endo*-cavity complexation of the alkyl chain. The absence of typical shielded benzylic resonances in the 4−6 ppm region was a clear-cut proof that *endo*-butyl-**4d**$^+\subset$**3** pseudo[2]rotaxane had been exclusively formed. DFT calculations[33] at the B3LYP/6-31G* level of theory were in good accordance with this result, indicating that the *endo*-butyl−**4d**$^+\subset$**3** stereoisomer was more stable than the *endo*-benzyl one by 3.1 kcal/mol (Figure 15). Of course, this result is perfectly in line with those of calix[6]arene wheels discussed above. The absence of *through-the-annulus* threading of butylbenzylammonium axle **4d**$^+$ with calix[8]arene wheel **2** can be explained by the smaller dimension of its 24-membered subcavities when compared to the larger 25-membered ones of **3**. Clearly, these latter can give a better accommodation of the bulkier butylbenzylammonium axle, which would be too tight inside those of wheel **2**. Of course, this result is in agreement with the above observed higher stability of pseudorotaxane based on **3** with respect to those derived by **2**.

CONCLUSION

In conclusion, we have shown that the *through-the-annulus* threading of the larger calix[8]arene macrocycle with di-*n*-alkylammonium threads occurs only upon partial rigidification of the calix[8]arene skeleton by intramolecular bridging. In particular, 1D and 2D NMR studies indicated that 1,5-bridged

dx.doi.org/10.1021/jo401206j | J. Org. Chem. 2013, 78, 7627−7638

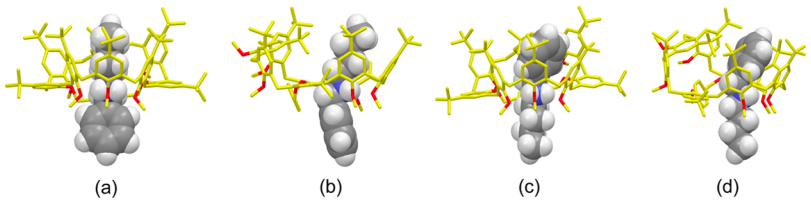

Figure 15. (a) Front and (b) side views of the energy-minimized structure of the *endo*-alkyl−**4d**$^+$⊂**3** pseudo[2]rotaxane stereoisomer. (c) Front and (d) side views of the energy-minimized structure of the *endo*-benzyl−**4d**$^+$⊂**3** pseudo[2]rotaxane stereoisomer (B3LYP DFT calculations using the 6-31G* basis set were used for both structures).

calix[8]arenes with a *meta*- or *para*-xylylene bridge (**2** and **3**) gave a 1:1 wheel/thread stoichiometry, in which one dialkylammonium axle was threaded into one of the two subcavities of the calix[8]-wheel. Conformational details about the structure adopted by the calix[8]arene wheel in pseudo[2]-rotaxane **4a**$^+$⊂**2** have been obtained by using chemical shift surface maps, previously reported by our group. Thus, a *syn* orientation was found for the contiguous triads of unbridged methylated rings (B−C−D and F−G−H rings) that give a 3/4-cone geometry, while an out orientation is adopted by the bridgehead A and E rings. The cooperative effect of the two subcavities in calix[8]arene wheels **2** and **3** leads to K_{ass} values for pseudorotaxane formation that were significantly higher than those obtained for the analogous threading with calix[6]arene host **1a**. In addition, 1,5-*p*-xylylene-bridged calix[8]-wheel **3** shows pseudo[2]rotaxane K_{ass} values higher than those of 1,5-*m*-xylylene-bridged analogue **2**. This result can be explained by the larger dimension of the 25-membered subcavity of **3**, over the 24-membered one of **2**, which can better accommodate the dialkylammonium axle. ^{1}H VT NMR studies confirmed that the thread templation in calix-pseudorotaxanes has an important role in the stabilization of cone-conformation of the calix-wheel. Indeed, a direct correlation was found between the host conformational stabilization defined by the energy barrier value ($\Delta G^{\ddagger}$) and the complex thermodynamic stability (ΔG_{ass}) derived from experimental association constants. Finally, an *endo*-alkyl oriented pseudo[2]rotaxane was obtained when calix[8]-wheel **3** was treated with the directional butylbenzylammonium thread **4d**$^+$. DFT-B3LYP/6-31G* calculations were in good accordance with this result, indicating that the *endo*-alkyl−**4d**$^+$⊂**3** stereoisomer was more stable than the *endo*-benzyl one by 3.1 kcal/mol.

EXPERIMENTAL SECTION

General Experimental Method. High-resolution ESI-MS spectra of each compound were performed on a Q-Tof mass spectrometer, equipped with an electrospray ion source. Each compound was analyzed by direct infusion using CH_2Cl_2/CH_3OH/HCOOH (80:18:2) as solvent. The instrument was calibrated using [Glu1]-Fibrinopeptide B. All chemicals were reagent grade and were used without further purification. Anhydrous solvents were used as purchased from the supplier. When necessary, compounds were dried in vacuo over $CaCl_2$. Reaction temperatures were measured externally. Derivatives **1a**,[38] **1b**,[23] **2**,[27] **3**,[27] **4d**$^+$·TFPB$^-$[19], and sodium tetrakis[3,5-bis(trifluoromethyl)-phenyl]borate[20b] were synthesized according to literature procedures. NMR spectra were recorded on a 400 MHz spectrometer; chemical shifts are reported relative to the residual solvent peak. One-dimensional ^{1}H and ^{13}C spectra, DEPT-90, DEPT-135, COSY-45, heteronuclear multiple-bond correlation (HMBC), heteronuclear single quantum correlation (HSQC), and ROESY were used for NMR peak assignment of **4a**$^+$⊂**2** pseudo[2]rotaxane. COSY-45 spectra were taken using a relaxation delay of 2 s with 30 scans and 170 increments of 2048 points each. HMBC spectra were performed without ^{1}H decoupling, with a low-pass J-filter to suppress one-bond correlations, and with a delay of 70 ms for the evolution of long-range couplings. The number of scans taken was 50, with 413 increments of 4096 points each. HSQC spectra were performed with gradient selection, sensitivity enhancement, and phase-sensitive mode using the Echo/Antiecho-TPPI procedure. A typical experiment comprised 20 scans with 113 increments of 2048 points each. ROESY spectra were recorded in phase-sensitive mode using a mixing time t_m of 200 ms. Molecular modeling studies were performed with a combined use of the MacroModel-9/Maestro-4.1 program and the Gaussian 09 software package.[39] Input structure files for DFT calculations were obtained by molecular modeling with the MacroModel 9.0 program (Schrödinger, LLC, New York, NY, 2005)[32] using the AMBER force field and $CHCl_3$ solvent (GB/SA model). The input structure files were optimized at the DFT B3LYP level of theory using the 6-31G* basis set for the entire system.

General Procedure for the Synthesis of Di-*n*-hexylammonium 4a$^+$ and Di-*n*-butylammonium 4c$^+$ Tetrakis[3,5-bis(trifluoromethyl)phenyl]borate (TFPB) Salts. A solution of sodium tetrakis[3,5-bis(trifluoromethyl)phenyl]borate[20b] (0.67 mmol) in dry methanol (2 mL) was added to the solution of appropriate dialkylammonium chloride salts (0.52 mmol) in dry methanol (3 mL). The resulting solution was stirred overnight. After removing methanol by evaporation, deionized water was added and the brown solid was filtered off and dried under vacuum for 24−48 h.

4a·TFPB$^-$ (0.49 g, 0.47 mmol, 90%). ESI−MS m/z = 186.2 [M − TFPB$^-$]$^+$; ^{1}H NMR ($CDCl_3$, 250 MHz, 298 K) δ 0.83 (t, CH_3CH_2−, J = 6.7 Hz, 6H), 1.24 (br s, overlapped, 12H), 1.52 (m, 4H), 2.94 (t, −$CH_2NH_2^+CH_2$−, J = 7.8 Hz, 4H), 7.57 (br s, ArH^{TFPB}, 4H), 7.71 (br s, ArH^{TFPB}, 8H); ^{1}H NMR (CD_3OD, 250 MHz, 298 K) δ 0.87 (br t, CH_3CH_2−, 6H), 1.32 (br s, overlapped, 12H), 1.62 (m, 4H), 2.92 (t, −$CH_2NH_2^+CH_2$−, J = 7.8 Hz, 4H), 7.55 (br s, ArH^{TFPB}, 12H); ^{13}C NMR (CD_3OD, 75 MHz, 298 K) δ 14.2, 23.4, 27.2, 27.3, 32.4, 118.4, 123.6, 127.9, 130.2, 130.6, 135.8. Anal. Calcd for $C_{44}H_{40}BF_{24}N^+$: C, 50.35; H, 3.84. Found: C, 50.26; H, 3.93.

4c·TFPB$^-$ (0.44 g, 0.44 mmol, 85%). ESI−MS m/z = 130.3 [M − TFPB$^-$]$^+$; ^{1}H NMR (CD_3OD, 400 MHz, 298 K) δ 0.98 [t, $(CH_3CH_2CH_2CH_2)_2NH_2^+$, J = 6.9 Hz, 6H], 1.40 [m, $(CH_3CH_2CH_2CH_2)_2NH_2^+$, 4H], 1.64 [m, $(CH_3CH_2CH_2\ CH_2)_2NH_2^+$, 4H], 2.98 [t, $(CH_3CH_2CH_2CH_2)_2NH_2^+$, J = 7.8 Hz, 4H], 7.60 (br s, ArH^{TFPB}, 12 H); ^{13}C NMR (CD_3OD, 75 MHz, 298 K) δ 15.0, 21.9, 30.5, 119.6, 120.1, 128.9, 131.7, 132.2, 137.2, 162.9, 163.7, 164.4, 165.1; Anal. Calcd for $C_{40}H_{32}BF_{24}N$: C, 48.36; H, 3.25. Found: C, 48.45; H, 3.16.

General Procedure for the Preparation of Calix[6,8]arene-Based Pseudo[2]rotaxanes. The calixarene derivative (1.23×10^{-3} mmol) and the appropriate alkylammonium TFPB salt **4a**−**4d**$^+$ (1.23×10^{-3} mmol) were dissolved in $CDCl_3$ (0.4 mL, 3.0×10^{-3} M solution). Each solution was sonicated for 15 min at room temperature and then was transferred into a NMR tube for 1D and 2D NMR spectra acquisition.

Determination of K_{ass} Values by Quantitative ^{1}H NMR Analysis.[35] The samples were prepared by dissolving the calixarene host (1.24×10^{-3} mmol) and the appropriate alkylammonium guest TFPB salt **4a**−**4d**$^+$ (1.24×10^{-3} mmol) in $CDCl_3$ (0.4 mL) containing 1 μL of 1,1,2,2-tetrachloroethane (d = 1.59 g/mL) as internal standard. The complex concentration [complex] was evaluated by integration of the ^{1}H NMR signal of $CHCl_2CHCl_2$ versus the shielded signals at negative values of the guest molecule. The following equation[35] was used to obtain the moles of the complex

dx.doi.org/10.1021/jo401206j | J. Org. Chem. 2013, 78, 7627−7638

$$\frac{G_a}{G_b} = \frac{F_a}{F_b} \times \frac{N_b}{N_a} \times \frac{M_a}{M_b}$$

where:

G_a = grams of 1,1,2,2-tetrachloroethane; G_b = grams of complex.
F_a and F_b = areas of the signals of 1,1,2,2-tetrachloroethane and shielded signal of the guest.
N_a and N_b = numbers of nuclei that cause the signals (N_a for 1,1,2,2-tetrachloroethane; N_b for guest).
M_a and M_b = molecular masses of 1,1,2,2-tetrachloroethane (a) and complex (b).

■ ASSOCIATED CONTENT

Supporting Information

^{1}H NMR spectra of new compounds **4a**$^+$ and **4b**$^+$, ESI(+) mass spectra and 2D NMR spectra of pseudo[2]rotaxanes, and assessment of the conformation of **2** in pseudo[2]rotaxane **4a**$^+$⊂**2** through chemical shift contour plots. This material is available free of charge via the Internet at http://pubs.acs.org.

■ AUTHOR INFORMATION

Corresponding Author

*E-mail: cgaeta@unisa.it (C.G.), neri@unisa.it (P.N.).

Notes

The authors declare no competing financial interest.

■ ACKNOWLEDGMENTS

We thank the Italian MIUR (PRIN 20109Z2XRJ_006) for financial support.

■ REFERENCES

(1) Sauvage, J. P., Dietrich-Buchecker, C., Eds. *Molecular Catenanes, Rotaxanes and Knots: A Journey Through the World of Molecular Topology*;Wiley-VCH: Weinheim, 1999.

(2) (a) Ikeda, T.; Saha, S.; Aprahamian, I.; Leung, K. C.-F.; Williams, A.; Deng, W.-Q.; Flood, A. H.; Goddard, W. A., III; Stoddart, J. F. *Chem.—Asian J.* **2007**, *2*, 76−93. (b) Collier, C. P.; Mattersteig, G.; Wong, E. W.; Luo, Y.; Beverly, K.; Sampaio, J.; Raymo, F. M.; Stoddart, J. F.; Heath, J. R. *Science* **2000**, *289*, 1172−1175.

(3) (a) Balzani, V.; Credi, A.; Venturi, M. *Molecular Devices and Machines*, 2nd ed.; Wiley-VCH: Weinheim, 2008. (b) Saha, S.; Stoddart, J. F. *Chem. Soc. Rev.* **2007**, *36*, 77−92.

(4) Caballero, A.; Zapata, F.; White, G. N.; Costa, P. J.; Felix, V.; Beer, P. D. *Angew. Chem., Int. Ed.* **2012**, *51*, 1876−1880.

(5) (a) Hoss, R.; Vögtle, F. *Angew. Chem., Int. Ed. Engl.* **1994**, *33*, 375−384. (b) Diederich, F., Stang, P. J., Eds. *Templated Organic Synthesis*; Wiley-VCH: Weinheim, 1999.

(6) (a) Gokel, G. W. *Crown Ethers and Cryptands*; Monographs in Supramolecular Chemistry; The Royal Society of Chemistry: Cambridge, U.K., 1991. For a recent report, see: (b) Fahrenbach, A. C.; Hartlieb, K. J.; Sue, C.-H.; Bruns, C. J.; Barin, G.; Basu, S.; Olson, M. A.; Botros, Y. Y.; Bagabas, A.; Khdary, N. H.; Stoddart, J. F. *Chem. Commun.* **2012**, *48*, 9141−9143.

(7) Special issue on cyclodextrins: (a) D'Souza, V. T.; Lipkowitz, K. B. *Chem. Rev.* **1998**, *98*, 1741−2076. (b) Lim, C. W.; Sakamoto, S.; Yamaguchi, K.; Hong, J.-I. *Org. Lett.* **2004**, *6*, 1079−1082. (c) Armspach, D.; Ashton, P. R.; Ballardini, R.; Balzani, V.; Godi, A.; Moore, C. P.; Prodi, L.; Spencer, N.; Stoddart, J. F.; Tolley, M. S.; Wear, T. J.; Williams, D. J. *Chem.—Eur. J.* **1995**, *1*, 33−55.

(8) (a) Park, K.-M.; Kim, S.-Y.; Heo, J.; Whang, D.; Sakamoto, S.; Yamaguchi, K.; Kim, K. *J Am. Chem. Soc.* **2002**, *124*, 2140−2147. (b) Lagona, J.; Mukhopadhyay, P.; Chakrabarti, S.; Isaacs, L. *Angew. Chem., Int. Ed.* **2005**, *44*, 4844−4870.

(9) (a) Leigh, D. A.; Wong, J. K. Y.; Dehez, F.; Zerbetto, F. *Nature* **2003**, *424*, 174−179. (b) Hernandez, J. V.; Kay, E. R.; Leigh, D. A. *Science* **2004**, *306*, 1532−1537. (c) White, N. G.; Beer, P. D. *Chem. Commun.* **2012**, *48*, 8499−8501. (d) Leigh, D. A.; Lusby, P. J.; Slawin, A. M. Z.; Walker, D. B. *Chem. Commun.* **2012**, *48*, 5826−5828.

(10) For comprehensive reviews on calixarene macrocycles, see: (a) Gutsche, C. D. *Calixarenes: An Introduction*; Royal Society of Chemistry: Cambridge, UK, 2008; Chapter 5, pp 116−128. (b) Asfari, Z., Böhmer, V., Harrowfield, J., Vicens, J., Eds. *Calixarenes 2001*; Kluwer: Dordrecht, 2001. (c) Böhmer, V. In *The Chemistry of Phenols*; Rappoport, Z., Ed.; Wiley: Chichester, UK, 2003; Chapter 19. (d) Vicens, J., Harrowfield, J., Eds. *Calixarenes in the Nanoworld*; Springer: Dordrecht, 2007.

(11) For general accounts, see ref 10, whereas for recent examples of chemical modification of calixarene macrocycles, see, for functionalization to bridging methylenes: (a) Columbus, I.; Biali, S. E. *Org. Lett.* **2007**, *9*, 2927−2929. For the introduction of oxygenated functions into the calix walls, see: (b) Troisi, F.; Mogavero, L.; Gaeta, C.; Gavuzzo, E.; Neri, P. *Org. Lett.* **2007**, *9*, 915−918. A novel approach to functionalize calixarene *exo-rim* with nucleophiles using calixarene *p*-bromodienone derivatives has been recently reported: (c) Troisi, F.; Pierro, T.; Gaeta, C.; Neri, P. *Org. Lett.* **2009**, *11*, 697−700. For a similar approach using calixarene spirodienones, see: (d) Thulasi, S.; Bhagavathy, G. V.; Eliyan, J. L.; Varma, R. *Tetrahedron Lett.* **2009**, *50*, 770−772.

(12) (a) Matthews, S. E.; Beer, P. D. In *Calixarenes 2001*; Asfari, Z., Böhmer, V., Harrowfield, J., Vicens, J., Eds.; Kluwer: Dordrecht, 2001; Chapter 23, pp 421−439. For recent examples, see: (b) Pinter, T.; Jana, S.; Courtemanche, R. J. M.; Hof, F. J. *Org. Chem.* **2011**, *76*, 3733−3741.

(13) (a) Abraham, W. *J. Inclusion Phenom. Macrocyclic Chem.* **2002**, *43*, 159−174. (b) Capici, C.; Cohen, Y.; D'Urso, A.; Gattuso, G.; Notti, A.; Pappalardo, A.; Pappalardo, S.; Parisi, M. F.; Purrello, R.; Slovak, S.; Villari, V. *Angew. Chem., Int. Ed.* **2011**, *50*, 11956−11961. (c) Le Gac, S.; Picron, J.-F.; Reinaud, O.; Jabin, J. *Org. Biomol. Chem.* **2011**, *9*, 2387−2396. (d) Monnereau, C.; Rebilly, J.-N.; Reinaud, O. *Eur. J. Org. Chem.* **2011**, 166−175.

(14) (a) Atwood, J. L.; Barbour, L. J.; Jerga, A. *Science* **2002**, *296*, 2367−2369. (b) Atwood, J. L.; Barbour, L. J.; Jerga, A. *Angew. Chem., Int. Ed.* **2004**, *43*, 2948−2950. (c) Canlas, C. P.; Lu, J.; Ray, N. A.; Grosso-Giordano, N. A.; Lee, S.; Elam, J. W.; Winans, R. E.; Van Duyne, R. P.; Stair, P. C.; Notestein, J. M. *Nat. Chem.* **2012**, *4*, 1030−1036.

(15) (a) Wyler, R.; de Mendoza, J.; Rebek, J., Jr. *Angew. Chem., Int. Ed. Engl.* **1993**, *32*, 1699−1701. (b) Meissner, R. S.; Rebek, J., Jr.; de Mendoza, J. *Science* **1995**, *270*, 1485−1488. (c) Mogck, O.; Paulus, E. F.; Boehmer, V.; Thondorf, I.; Vogt, W. *Chem. Commun.* **1996**, 2533−2534. (d) Conn, M. M.; Rebek, J., Jr. *Chem. Rev.* **1997**, *97*, 1647−1668. (e) MacGillivray, L. R.; Atwood, J. L. *Nature* **1997**, *389*, 469−472. (f) Prins, L. J.; De Jong, F.; Timmerman, P.; Reinhoudt, D. N. *Nature* **2000**, *408*, 181−184. (g) Kerckhoffs, J. M. C. A.; ten Cate, M. G. J.; Mateos-Timoneda, M. A.; Van Leeuwen, F. W. B.; Snellink-Rueel, B.; Spek, A. L.; Kooijman, H.; Crego-Calama, M.; Reinhoudt, D. N. *J. Am. Chem. Soc.* **2005**, *127*, 12697−12708. (h) Pasquale, S.; Sattin, S.; Escudero-Adán, E. C.; Martínez-Belmonte, M.; de Mendoza, J. *Nat. Commun.* **2012**, *1793*, 1−7.

(16) (a) Hong, B. H.; Bae, S. C.; Lee, C.-W.; Jeong, S.; Kim, K. S. *Science* **2001**, *294*, 348−351. (b) Atwood, J. L.; Barbour, L. J.; Jerga; Schottel, A. B. L. *Science* **2002**, *298*, 1000−1002.

(17) For the first example of through-the-annulus catenated calixarenes (calix[2]catenanes), see: (a) Gaeta, C.; Talotta, C.; Mirra, S.; Margarucci, L.; Casapullo, A.; Neri, P. *Org. Lett.* **2013**, *15*, 116−119. For recent examples of calixarene-based catenane systems in which the calixarene annulus is unthreaded, see: (b) Schlesier, T.; Metzroth, T.; Janshoff, A.; Gauss, J.; Diezemann, G. *J. Phys. Chem. B* **2011**, *115*, 6445−6454. (c) Phipps, D. E.; Beer, P. D. *Tetrahedron Lett.* **2009**, *50*, 3454−3457. (d) Li, Z.-T.; Zhao, X.; Shao, X.-B. In *Calixarenes in the Nanoworld*; Harrowfield, J.,Vicens, J., Eds.; Springer: Dordrecht, The Netherlands, 2007; Chapter 3, pp 47−62 and references cited therein. (e) Wang, L.; Vysotsky, M. O.; Bogdan, A.; Bolte, M.; Böhmer, V. *Science* **2004**, *304*, 1312−1314.

(18) (a) Arduini, A.; Ferdani, R.; Pochini, A.; Secchi, A.; Ugozzoli, F. *Angew. Chem., Int. Ed.* **2000**, *39*, 3453−3456. (b) Talotta, C.; Gaeta, C.; Pierro, T.; Neri, P. *Org. Lett.* **2011**, *13*, 2098−2101. (c) Pierro, T.; Gaeta,

C.; Talotta, C.; Casapullo, A.; Neri, P. *Org. Lett.* **2011**, *13*, 2650−2653. (d) Talotta, C.; Gaeta, C.; Neri, P. *Org. Lett.* **2012**, *14*, 3104−3107.
(19) Gaeta, C.; Troisi, F.; Neri, P. *Org. Lett.* **2010**, *12*, 2092−2095.
(20) (a) Strauss, S. H. *Chem. Rev.* **1993**, *93*, 927−942. (b) Nishida, H.; Takada, N.; Yoshimura, M.; Sonoda, T.; Kobayashi, H. *Bull. Chem. Soc. Jpn.* **1984**, *57*, 2600−2604. For recent examples on the use of TFPB superweak anion in supramolecular chemistry, see: (c) Han, C.; Gao, L.; Yu, G.; Zhang, Z.; Dong, S.; Huang, F. *Eur. J. Org. Chem.* **2013**, 2529−2532. (d) Chen, N.-C.; Chuang, C.-J.; Wang, L.-Y.; Lai, C.-C.; Chiu, S.-H. *Chem.—Eur. J.* **2012**, *18*, 1896−1900. (e) Li, C.; Shu, X.; Li, J.; Fan, J.; Chen, Z.; Weng, L.; Jia, X. *Org. Lett.* **2012**, *14*, 4126−4129. (f) Gaeta, C.; Talotta, C.; Farina, F.; Camalli, M.; Campi, G.; Neri, P. *Chem.—Eur. J.* **2012**, *18*, 1219−1230. (g) Gaeta, C.; Talotta, C.; Farina, F.; Teixeira, F. A.; Marcos, P. A.; Ascenso, J. R.; Neri, P. *J. Org. Chem.* **2012**, *77*, 10285−10293. (h) Blight, B. A.; Camara-Campos, A.; Djurdjevic, S.; Kaller, M.; Leigh, D. A.; McMillan, F. M.; McNab, H.; Slawin, A. M. *J. Am. Chem. Soc.* **2009**, *131*, 14116−14122. (i) Hou, H.; Leung, K. C.-F.; Lanari, D.; Nelson, A.; Stoddart, J. F.; Grubbs, R. H. *J. Am. Chem. Soc.* **2006**, *128*, 13358−13359. For a review on counterion effects in supramolecular chemistry, see: (j) Gasa, T. B.; Valente, C.; Stoddart, J. F. *Chem. Soc. Rev.* **2011**, *40*, 57−78.
(21) Gattuso, G.; Notti, A.; Parisi, M. F.; Pisagatti, I.; Amato, M. E.; Pappalardo, A.; Pappalardo, S. *Chem.—Eur. J.* **2010**, *16*, 2381−2385.
(22) For a review on calix[8]arene macrocycle, see: Neri, P.; Consoli, G. M. L.; Cunsolo, F.; Geraci, C.; Piattelli, M. In *Calixarenes 2001*; Asfari, Z., Böhmer, V., Harrowfield, J., Vicens, J., Eds.; Kluwer: Dordrecht, 2001; Chapter 5, pp 89−109.
(23) Consoli, G. M. L.; Cunsolo, F.; Neri, P. *Gazz. Chim. Ital.* **1996**, *126*, 791−798.
(24) See the Supporting Information for further details.
(25) Stewart, D. R.; Krawiec, M.; Kashyap, R. P.; Watson, W. H.; Gutsche, C. D. *J. Am. Chem. Soc.* **1995**, *117*, 586−601.
(26) Cunsolo, F.; Piattelli, M.; Neri, P. *J. Chem. Soc., Chem. Commun.* **1994**, 1917−1918.
(27) Gaeta, C.; Martino, M.; Gregoli, L.; Neri, P. *Tetrahedron Lett.* **2002**, *43*, 8875−8878.
(28) Gutsche, C. D.; Gutsche, A. E.; Karaulov, A. I. *J. Inclusion Phenom.* **1985**, *3*, 447−451.
(29) Czugler, M.; Tisza, S.; Speier, G. *J. Inclusion Phenom. Mol. Recognit. Chem.* **1991**, *11*, 323−331.
(30) Ferro, R.; Tedesco, T.; Gaeta, C.; Neri, P. *J. Inclusion Phenom. Macrocyclic Chem.* **2005**, *52*, 85−91.
(31) (a) Bifulco, G.; Gomez-Paloma, L.; Riccio, R.; Gaeta, C.; Troisi, F.; Neri, P. *Org. Lett.* **2005**, *7*, 5757−5760. (b) Bifulco, G.; Riccio, R.; Gaeta, C.; Neri, P. *Chem.—Eur. J.* **2007**, *13*, 7185−7194.
(32) MacroModel-9.0/Maestro-4.1 program: Mohamadi, F.; Richards, N. G.; Guida, W. C.; Liskamp, R.; Lipton, M.; Caufield, C.; Chang, G.; Hendrickson, T.; Still, W. C. *J. Comput. Chem.* **1990**, *11*, 440−467.
(33) DFT calculations were performed at the B3LYP level, using the 6-31G* basis set for the entire system (Gaussian 09 Software Package).
(34) This conclusion was based on Gutsche's "^{1}H NMR $\Delta\delta$" rule, which is based on the chemical shift difference of each pair of $ArCH_2Ar$ protons, which can be diasterotopic or homotopic for symmetry reasons, thus leading to AX (AB) or A2 systems, respectively. In particular, a ^{1}H NMR $\Delta\delta$ value of 0.7−1.0, or greater, indicates a *syn* orientation of the two corresponding proximal phenol rings as in the cone conformation, whereas a $\Delta\delta$ value close to zero (0.3−0.0) identifies an *anti* orientation between them, as in the 1,3-alternate conformation. Intermediate values of 0.5−0.3 ppm are usually attributed to an out or flattened orientation or to an averaged fast-exchanging conformation. See: (a) Gutsche, C. D. *Calixarenes*; Royal Society of Chemistry: Cambridge, U.K., 1989; pp 110−111. (b) Kanamathareddy, S.; Gutsche, C. D. *J. Org. Chem.* **1992**, *57*, 3160−3166.
(35) (a) Hirose, K. In *Analytical Methods in Supramolecular Chemistry*; Schalley, C. A., Ed.; WILEY-VCH: Weinheim, 2007; Chapter 2, pp 17−54. (b) Braun, S., Kalinowsky, H.-O., Berger, S., Eds. *150 and More Basic NMR Experiments: A Practical Course*; WILEY-VCH: Weinheim; 1996; pp 232−233.
(36) (a) Neri, P.; Bottino, A.; Cunsolo, F.; Piattelli, M. *Angew. Chem., Int. Ed.* **1998**, *37*, 166−169. (b) Fasting, C.; Schalley, C. A.; Weber, M.; Seitz, O.; Hecht, S.; Koksch, B.; Dernedde, J.; Graf, C.; Knapp, E.-W.; Haag, R. *Angew. Chem., Int. Ed.* **2012**, *51*, 10472−10498. (c) Jiang, K. N. W.; Löw, N. L.; Dzyuba, E. V.; Klautzsch, F.; Schäfer, A.; Huuskonen, J.; Rissanen, K.; Schalley, C. A. *J. Am. Chem. Soc.* **2012**, *134*, 1860−1868.
(37) Talotta, C.; Gaeta, C.; Qi, Z.; Schalley, C. A.; Neri, P. *Angew. Chem., Int. Ed.* **2013**, *52*, 7437−7441.
(38) Chang, S.-K.; Cho, I. *J. Chem. Soc., Perkin Trans 1* **1986**, 211−214.
(39) Frisch, M. J.; Trucks, G. W.; Schlegel, H. B.; Scuseria, G. E.; Robb, M. A.; Cheeseman, J. R.; Scalmani, G.; Barone, V.; Mennucci, B.; Petersson, G. A.; Nakatsuji, H.; Caricato, M.; Li, X.; Hratchian, H. P.; Izmaylov, A. F.; Bloino, J.; Zheng, G.; Sonnenberg, J. L.; Hada, M.; Ehara, M.; Toyota, K.; Fukuda, R.; Hasegawa, J.; Ishida, M.; Nakajima, T.; Honda, Y.; Kitao, O.; Nakai, H.; Vreven, T.; Montgomery, J. A., Jr.; Peralta, J. E.; Ogliaro, F.; Bearpark, M.; Heyd, J. J.; Brothers, E.; Kudin, K. N.; Staroverov, V. N.; Kobayashi, R.; Normand, J.; Raghavachari, K.; Rendell, A.; Burant, J. C.; Iyengar, S. S.; Tomasi, J.; Cossi, M.; Rega, N.; Millam, J. M.; Klene, M.; Knox, J. E.; Cross, J. B.; Bakken, V.; Adamo, C.; Jaramillo, J.; Gomperts, R.; Stratmann, R. E.; Yazyev, O.; Austin, A. J.; Cammi, R.; Pomelli, C.; Ochterski, J. W.; Martin, R. L.; Morokuma, K.; Zakrzewski, V. G.; Voth, G. A.; Salvador, P.; Dannenberg, J. J.; Dapprich, S.; Daniels, A. D.; Farkas, Ö.; Foresman, J. B.; Ortiz, J. V.; Cioslowski, J.; Fox, D. J. *Gaussian 09*, Revision A.1; Gaussian, Inc.: Wallingford, CT, 2009.